Neutrino Mass and Mixing Measurements at Super-Kamiokande

R. Svoboda (for the Super-Kamiokande Collaboration) [a]

[a]Department of Physics and Astronomy, Louisiana State University,
Baton Rouge, LA 70803-4001 USA

The latest atmospheric and solar neutrino measurements from over 1100 live days of the Super-Kamiokande detector are presented. Atmospheric results continue to strongly support the hypothesis of ν_μ oscillations via the measured deficit of $\mu - like$ interactions and the strong dependence of the deficit on neutrino flight distance. Analysis of the data gives best fit 2-component oscillation parameters $(\sin^2 2\theta,\ \delta m^2) = (1.00, 3.2 \times 10^{-3} ev^2)$ with $\chi^2/DOF = 124.7/135$. In contrast, the no-oscillation hypothesis gives $\chi^2/DOF = 296.5/139$. For solar neutrinos, no evidence of neutrino oscillations is seen in the spectral shape or expected day/night enhancement effect. The Small Mixing Angle (SMA) and Vacuum Oscillation (VO) allowed regions from flux deficit alone are excluded at the 95% *c.l.*

1. The Super-Kamiokande Detector

The Super-Kamiokande detector is a 50 kton (22.4 kton fiducial) water Cherenkov detector located in the Kamioka Mine near Toyama, Japan. consists of 11,134 50-cm photomultiplier tubes (PMT's) mounted in a cylindrical steel cage facing inwards. These PMT's record the leading edge and integrated pulse height from Cherenkov light produced by the passage of relativistic particles through the water. This information is used to deduce the vertex, direction, and deposited energy of the particle tracks. In addition, the characteristic ring pattern produced by Chernkov light is used to identify electrons and gammas from heavier charged particles such as muons, pions, and protons.

Energy calibration of Super-Kamiokande is performed using several independent techniques, including muon decay electrons, muon dE/dx, an electron LINAC, and ^{16}N decay from a deuterium-tritium (DT) neutron generator. The absolute energy scale is known to 2.5% at high energy ($> 100 MeV$) and to 1% at low energy (where the LINAC comes into play). Particle identification has been checked using a 1 kton prototype and a test beam at the KEK accelerator and is known to be accurate to within a few percent. Further details on detector construction and calibration have been published elsewhere. [1–3]

Super-Kamiokande was built primarily to make precision measurements of the flux of atmospheric and solar neutrinos and to search for proton decay with an order-of-magnitude more sensitivity than previous experiments. We have now analyzed over 1100 days of which is reported on in a preliminary fashion here.

2. Atmospheric Neutrinos

Since the initial evidence for strong evidence for neutrino oscillations was published in 1998 [1] Super-Kamiokande has continued to collect data from atmospheric neutrinos, now reaching 1144 days. New results continue to strengthen the oscillation interpretation of the deficit of ν_μ CC interactions and imply that the oscillation is likely to be $\nu_\mu \rightarrow \nu_\tau$. This evidence comes consistently from three independent neutrino data samples: (1) Fully Contained (FC) events in which all charged tracks begin and end inside the inner detector, (2) Partially-Contained (PC) events, in which one or more tracks (almost always muons) leave the detector, and (3) Upward-Going Muons (UGM), in which the interaction vertex is in the rock outside the detector. Analysis of these three

samples are described below.

2.1. Analysis of the Fully-Contained and Partially-Contained Sample

For the FC sample, neutrino-induced events are divided into 1, 2, or ≥ 3 or ring events (indicating the number of measured particle tracks above Cerenkov threshold) as shown in table 1. In order to measure the relative contributions of ν_μ and ν_e events to this sample, the one-ring events are used, since this sample is expected to be $> 90\%$ charged-current (CC).

Table 1
1144-day Atmospheric Neutrino Sample

number of rings	DATA	MC
1R	6344	7548
2R	1765	2135
$\geq$ 3R	1318	1657
Total	9427	11340

These one-ring events are further divided into $e-like$ amd $\mu-like$ based on a maximum likelihood particle ID technique which uses the "showering" and "non-showering" nature of electron and muon tracks, respectively. This ID technique has been fully tested in a test-beam experiment at KEK and is better than 99% accurate for single lepton tracks. A momentum cut is then made at 100 MeV/c if the event is $e-like$ and 200 MeV/c if the event is $\mu-like$. This is to give both muons and electrons roughly the same visible energy threshold in a water detector. This data sample is summarized in table 2. Also included are the predictions from two models, that of Honda [4] and that of Gaisser et al [5]. PC events are also shown.

Table 2: Particle Identification of Single-Ring Events

	DATA		Honda		Gaisser *et al.*	
	$e-like$	$\mu-like$	$e-like$	$\mu-like$	$e-like$	$\mu-like$
$E_{vis} < 1.33\,GeV$	2531	2486	2403	3621	2365	3515
$E_{vis} > 1.33\,GeV$	576	502	555	739	576	739
Part. Contained	0	665	0	945	0	997

Although the *absolute* rate of events is uncertain to roughly 20%, the *ratio* of ν_μ to ν_e is known to about 8% for the sub-GeV

($E_{vis} < 1.33\,GeV$) sample and 12% for the multi-GeV ($E_{vis} > 1.33\,GeV$) sample, since it is mostly determined by π decay kinematics. Since the 1-ring events are mostly CC, the $e-like$ events are highly correlated with ν_e (87%) and the $\mu-like$ events are likewise correlated with ν_μ (95%). Comparing the ratio of $\mu-like$ to $e-like$ in the data with the predictions from the Honda model gives:

$$\frac{(\mu/e)_{DATA}}{(\mu/e)_{MC}} = 0.652 \pm 0.019(stat) \pm 0.051(sys) \quad (1)$$
$$(E_{vis} < 1.33\,GeV)$$

$$\frac{(\mu/e)_{DATA}}{(\mu/e)_{MC}} = 0.668 \pm 0.035(stat) \pm 0.079(sys) \quad (2)$$
$$(E_{vis} > 1.33\,GeV\ +\ PC)$$

Similar results hold for the Gaisser model. This ratio shows a distinct zenith angle dependence that is well-fit by a $\nu_\mu \rightarrow \nu_\tau$ oscillation hypothesis. As expected, this dependence becomes more distinct at higher energies since the charged lepton track is more closely aligned with that of the parent neutrino, which means $\frac{L}{E}$ is better determined. This can be seen by slowly increasing the energy. Figures 1 2 3 show the zenith angle dependence of $R = \frac{(\mu/e)_{DATA}}{(\mu/e)_{MC}}$ for events with momentum < 400 MeV/c, for > 400 MeV/c, and for the multi-GeV ($E_{vis} > 1.33 GeV$) sample combined with the PC sample.

The zenith angle dependence and R-values tightly constrain the oscillation parameters for $\nu_\mu \rightarrow \nu_\tau$ Figure 4 shows the confidence level contours in δm^2 and $\sin^2 2\theta$ at 68%, 95%, and 99% intervals. The best fit value is $(\sin^2 2\theta, \delta m^2) = (1.00, 3.2 \times 10^{-3} ev^2)$ and has $\chi^2/DOF = 124.7/135$. In contrast, the no-oscillation fit has $\chi^2/DOF = 296.5/139$.

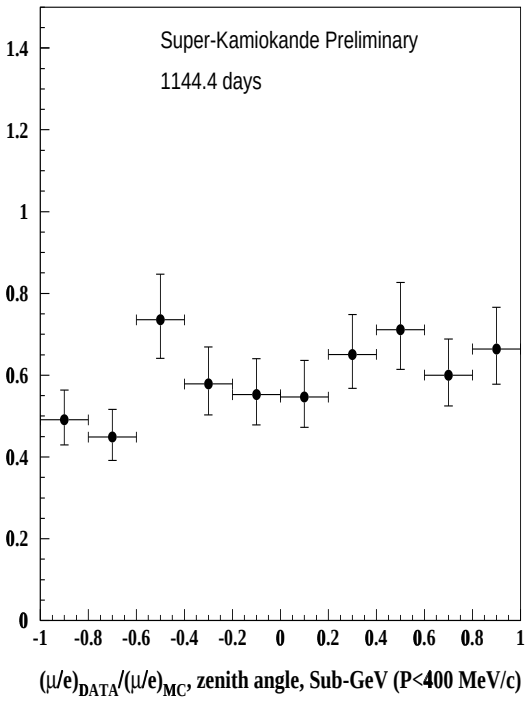

Figure 1. Zenith angle distribution of R for events with $P < 400\,MeV/c$.

2.2. Analysis of the Upward-Going Muon Sample

In the analysis of the UGM sample, the data are divided into two classes, stopping and through-going. The stopping muons are generated by ν_μ with a typical energy of around 10 GeV while the through-going come from energies around 100 GeV. At these energies, geomagnetic effects are minimal and the muon follows the path of the neutrino to with a few degrees. These muons can be used to test for oscillations by comparing the shape of the angular distribution against predictions. Table 3 shows the measured number of events as compared with expectations.

Figure 5 shows the zenith angle distribution of through-going muons. The horizon is at $\cos\theta_z = 0$. The solid line shows the expected distribution from the flux calculation of Gaisser

Table 3
1138(through) and 1117(stopped) live day upward-going muon sample.

sample name	number events	flux ($\times 10^{-13} cm^{-2} s^{-1} sr^{-1}$) measured	Honda	Bartol
through-going	1269	$1.70 \pm .05$	1.84 ± 0.41	1.97 ± 0.44
stopped	311	$0.41 \pm .04$	0.68 ± 0.15	0.73 ± 0.16

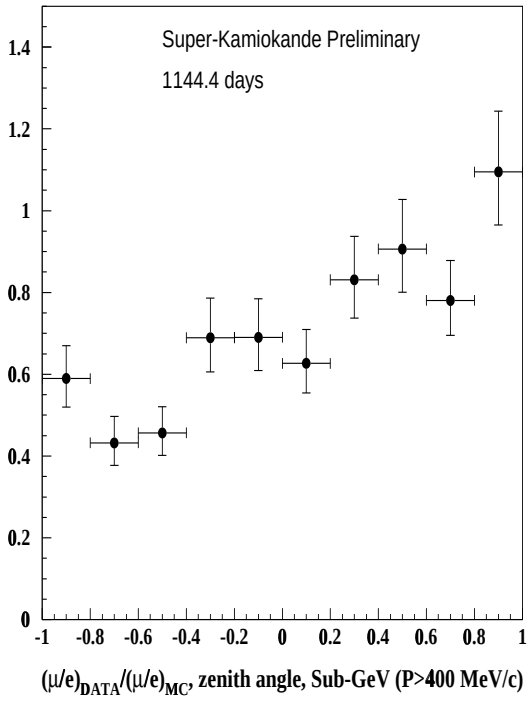

Figure 2. Zenith angle distribution of R for events with $P > 400\ MeV/c$.

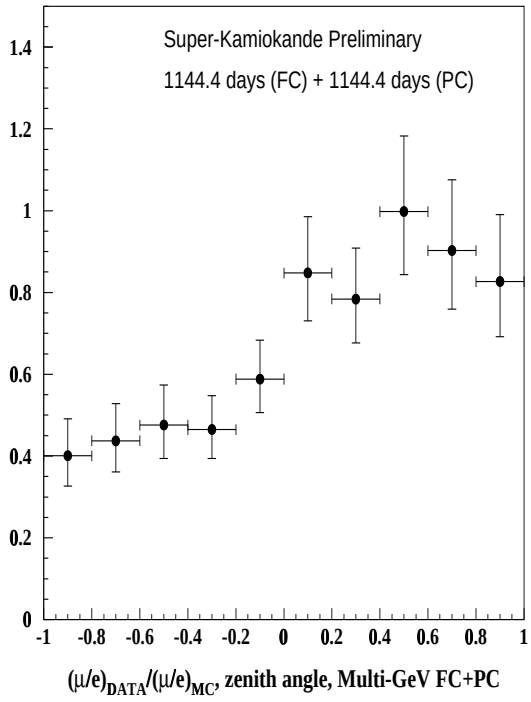

Figure 3. Zenith angle distribution of R for the multi-Gev+PC sample.

st al. [5]. Although the absolute value of the total flux is not so different from expectation, the agreement is very poor for the *shape* of the distribution, with $\chi^2/DOF = 22.6/10$.

Figure 6 shows a similar plot, but for the ratio between the upward-going stopped and through-going muons. This ratio is more sensitive to oscillations than a direct flux comparision since many of the systematic errors having to do with the input cosmic ray flux cancel. It can be seen that the value of the ratio is much lower than expected, implying that low energy stopping muons are being systematically suppressed. This is consistent with the oscillation picture deduced from the analysis of the contained events. Indeed, the best fit oscillation parameters from the UGM analysis alone (combined through-going and stopped muons) are $(\delta m^2, \sin^2 2\theta) = (1.0, 3.2 \times 10^{-3})$. This is quantitatively consistent with the values from the contained analysis. The dashed histograms in figures 5 and 6 show the distri-

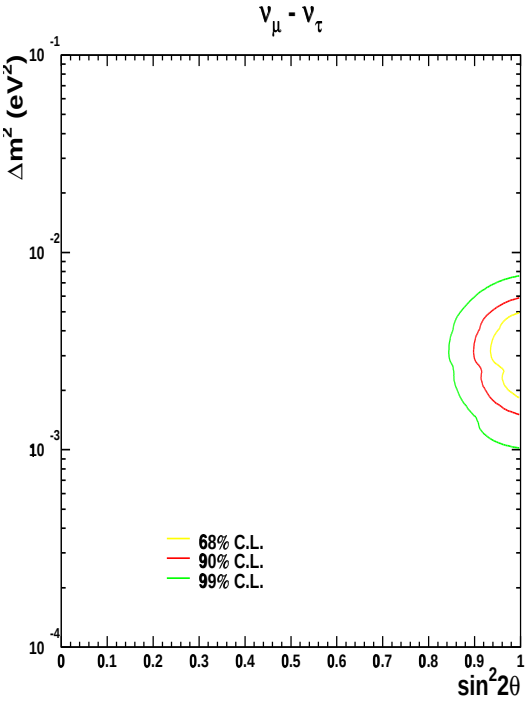

Figure 4. Confidence level contours for $\nu_\mu \rightarrow \nu_\tau$ oscillations using the FC and PC sample.

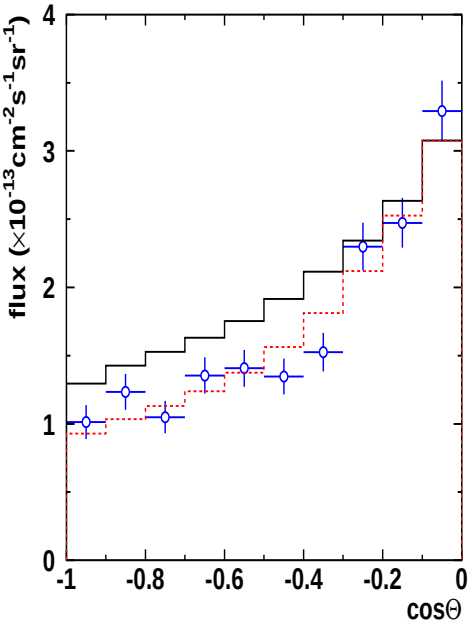

Figure 5. Zenith angle distribution of upward through-going muons. The solid curve is the expected distribution with no oscillations, while the dashed curve is the expectation with the best fit oscillation parameters from the UGM data alone $(\delta m^2, \sin^2 2\theta) = (1.0, 3.2 \times 10^{-3})$
.

butions expected from the neutrino oscillation hypothesis with these parameters. For this hypothesis $\chi^2/DOF = 13.0/13$, so both the UGM through-going angular distribution and the stopping muon ratio as a function of angle are well reproduced by disappearance due to oscillations.

3. Oscillation to Sterile versus Active Neutrinos

Atmospheric neutrino measurements continue to provide strong evidence that we are seeing the oscillation of muon neutrinos, most likely to tau neutrinos, but in addition, studies on a NC enriched sample of multi-ring events and on matter effects in high energy (> 5 GeV) ν_μ - ν_s mixing have strongly disfavored oscillation to sterile neutrinos as a solution to the Atmospheric Neutrino Problem [6,7]. This analysis, which used the same data set of this paper, has already been published [8]. Such neutrinos have been suggested as a way to reconcil SK and LSND [9] results.

4. Solar Neutrinos

The solar neutrino recoil electron spectrum at high energy continues to flatten; especially after divising new spallation cuts that reduce the background by a factor of two, and shifting the absolute energy scale by 0.3% based on new LINAC and DT data. This has resulted in

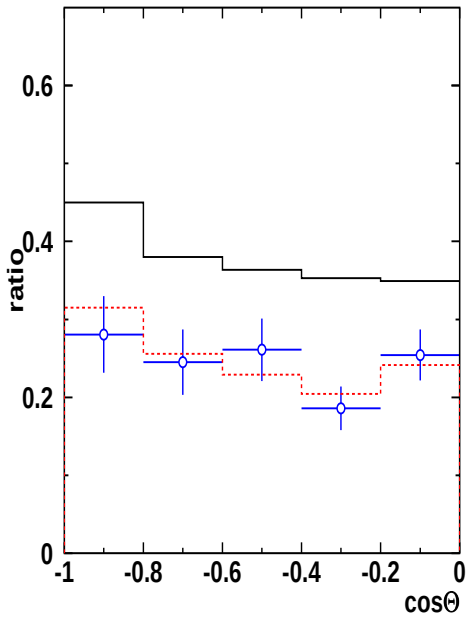

Figure 6. Zenith angle distribution of upward stopped muons. The solid curve is the expected distribution with no oscillations, while the dashed curve is the expectation with the best fit oscillation parameters from the UGM data alone $(\delta m^2, \sin^2 2\theta) = (1.0, 3.2 \times 10^{-3})$
.

a smaller fitted possible contribution from *hep* * and a better fit to an undistorted spectrum. This, coupled with the new lower threshold (5.0 MeV) has resulted in greater sensitivity for the type of spectral distortions produced by the SMA and vacuum solutions to the Solar Neutrino Problem [10–12,?]. As a consequence, these solutions are now disfavored at more than 95% c.l.

4.1. Absolute Flux

To extract the flux of solar neutrinos, the direction of contained events with energy < 5 MeV are compared with that of the sun at the time of detection. Figure 7 shows distribution of the cosine of the angle to the sun.

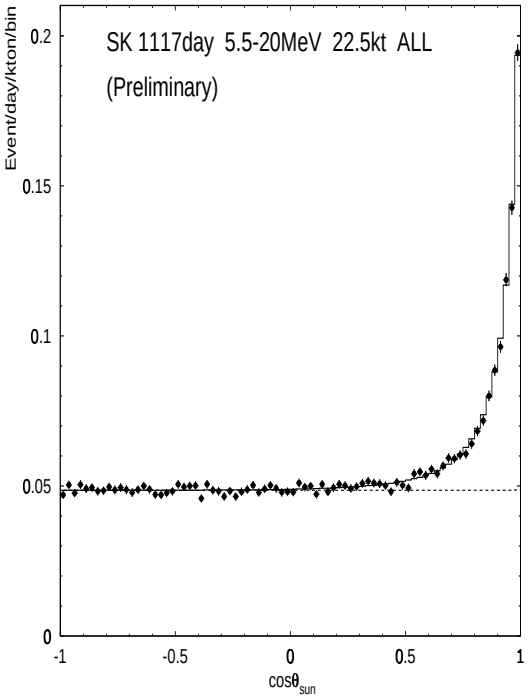

Figure 7. Distribution of the angle from the sun of contained events in the energy range 5.5-20 MeV for 1117 days of observation.

The shape of these angular distributions fits well to a flat background with a signal of neutrino-electron scattering events from the solar direction. The total solar neutrino signal can be extracted by doing a maximum liklihood fit to give a solar neutrino induced recoil event rate of about 14 events/day. Assuming a pure ^8B spectrum) this translates into a ^8B flux from the sun of:

$$2.40 \pm 0.03(stat.)^{+0.08}_{-0.07}(sys.) \times 10^6 cm^{-2} s^{-1} \quad (3)$$

Comparison with the BP98 Standard Solar

*$^3He + p \rightarrow ^4He + e^+ + \nu_e$

Model (*SSM*) [14] flux gives a ratio of data to *SSM* of:

$$\frac{Data}{SSM} = 0.465^{+0.005}_{-0.007}(stat.)^{+0.015}_{-0.013}(sys.) \quad (4)$$

The absolute flux data shows no significant variation with time over the last four years and continues to be consistent with a deficit when compared to expectations. Of course, the *raison d'etre* of Super-Kamiokande is the ability to: (1) look for spectral distortions in the recoil electron spectrum, as could result from several possible neutrino oscillation scenarios; (2) make a high-statistics division of the data into Day and Night subsets to look for neutrino regeneration in the Earth from an MSW-type mechanism; and (3) look for long-term seasonal variations in the flux as might be expected from some vacuum oscillation scenarios.

4.2. Energy Spectrum

The energy spectrum of recoil electrons can be extracted by simply dividing the data into bins of "visible energy" and doing the same signal extraction procedure bin-by-bin. The "visible energy" in this case is the total energy of the recoil electron corrected for Cerenkov threshold, water transparency, and PMT efficiency. The finite resolution of the detector has not been taken out (this can only be done by a model-dependent, statistical unfolding technique - and we want our results to not depend on any specific model). This means that a 10 MeV electron could result in a visible energy distributed in a roughly Gaussian shape centered on 10 MeV. The width of the distribution is dominated by counting statistics (we collect roughly 6.5 photoelectrons/MeV). Figure 8 shows the visible energy spectrum from the sun divided by the MC expectation. Except for the high-energy end above 12 MeV, most of the spectrum matches expectations quite well as regards *shape*. The fit to flat gives $\chi^2/DOF = 13.67/17$ for a confidence level of 69%.

The *hep* [†] reaction has an endpoint of 18 MeV and has been suggested as a possible cause for the rise at the end of the spectrum. hor our data, the best fit *hep* contribution was 5.4 ± 4.6 times the BP98 prediction. A new calculation of the cross-section for this reaction [15] predicts a value of 4.6 ± 0.3 and is consistent with our measurement. Nevertheless, we will continue to consider *hep* neutrinos as a possible source of excess high energy events of unknown normalization by making the relative normalization between ^8B and *hep* a free parameter in our oscillation analysis. Figure 8 shows the expected contribution from *hep* flux 4.6 times the BP98 prediction.

4.3. Day-Night Effect

Figure 9 shows the division of the 1117-day LE data into Day (545 days) and Night (572 days) subsets. The Small Angle MSW solution to the solar neutrino problem predicts an increase of the flux of neutrinos passing through the core and this is not seen. The asymmetry parameter α $(= (D - N)/\frac{1}{2}(D + N))$ is measured to be $-0.034 \pm 0.022 \pm 0.013$. The Large Angle solution would predict an overall broad increase in the night flux but only a small 1.3σ asymmetry seen, not enough to be significant.

4.4. Oscillation Analysis

We can use the non-observation of significant spectral distortions or day/night variations to set limits on neutrino oscillations. In all cases we will assume that the *hep* flux normalization is a free parameter.

Figures 10 shows the allowed regions of the MSW and Vacuum regions of oscillation parameter space allowed by using the absolute flux measured by SK and the gallium and chlorine experiments and comparing to expectations from BP98. Figure 11 shows the excluded regions based on non-observation of significant spectral distortion or day/night effects. The 95% exclusion regions cover the allowed SMA and Vacuum solutions completely, making them strongly dis-

[†] $^3He + p \rightarrow ^4He + e^+ + \nu_e$

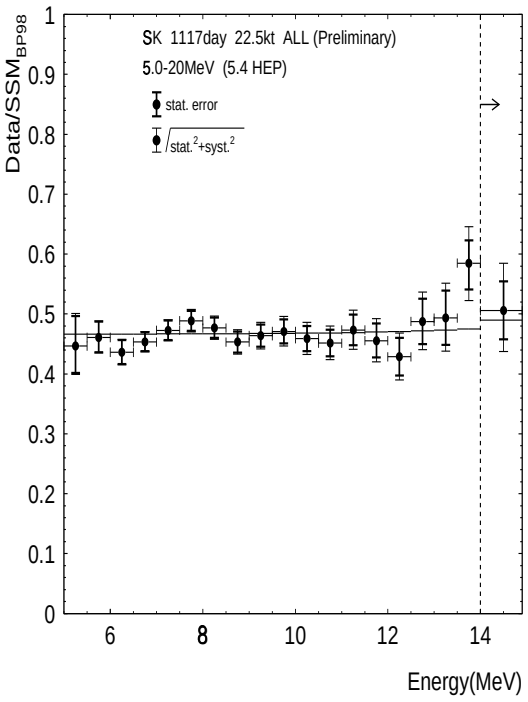

Figure 8. Total energy distribution for solar neutrino-induced recoil electrons in the energy range 5.0-20 MeV for 1117 days of observation. The data is divided by a Standard Solar Model (BP98) expectation. The solid line shows the result of assuming a contribution of *hep* neutrinos of 4.6 times the BP98 prediction.

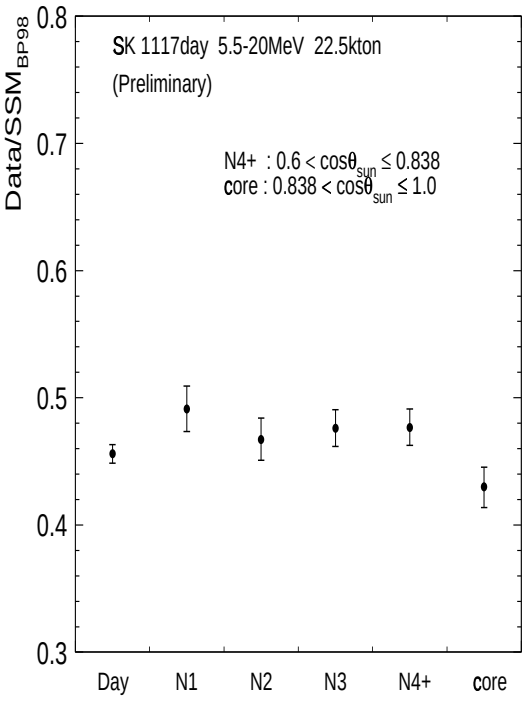

Figure 9. Comparison of Day and Night event rates in the energy range 5.5-20 MeV for 1117 days of observation.

favored.

5. Conclusions

Atmospheric neutrino data from Super-Kamiokande continues to strongly favor $\nu_\mu \to \nu_\tau$ ocsillations over the no oscillation hypothesis and oscillation to a sterile neutrino. This effect is confirmed at all energies and with 5 independent data sets. A strong correlation with neutrino flight distance is also seen in addition to simple ν_μ disappearance.

For solar neutrinos, there is no flux-independent indicators of neutrino oscialltions in the energy spectrum or time variation. Two of the four allowed regions (LMA and Vacuum) are rules out at the 95% c.l. by these measurements.

REFERENCES

1. Y.Fukuda *et al.*, *Phys. Rev. Lett.* **81**, 1562 (1998).
2. M.Nakahata *et al.*, *N.I.M.* A (1999).
3. E.Blaufuss *et al.*, submitted to *N.I.M.* A (2000).
4. M.Honda at al., Phys. Rev. D **52**, 4985 (1995).
5. V.Agrawal *et al.*, Phys. Rev, D **53** (1996).
6. T.J.Haines *et al.*, *Phys. Rev. Lett.* **57**, 1986

(1986).

7. K.S.Hirata *et al.*, *Phys. Lett.* **B205**, 416 (1988).

8. S.Fukuda *et al.*, *Phys. Rev. Lett.* **86** (2000).
9. C.Athanassopoulos, *et al.*, *Phys. Rev. Lett.* **81**, 1774 (1998).
10. B.T.Cleveland *et al.*, *Nucl. Phys.* B **38**, 47 (1995).
11. Y.Fukuda *et al.*, *Phys. Rev. Lett.* **77**, 1683 (1996).
12. J.N.Abdurashitov *et al.*, *Phys. Lett.* B **328**, 234 (1994).
13. P.Anselmann *et al.*, *Phys. Lett.* B **342**, 440 (1995).
14. J.N.Bahcall, S.Basu, and M.Pinsonneault, astro-ph/9805135.
15. L.E.Marcucci, *et al.* nucl-th/0006005 (2000).

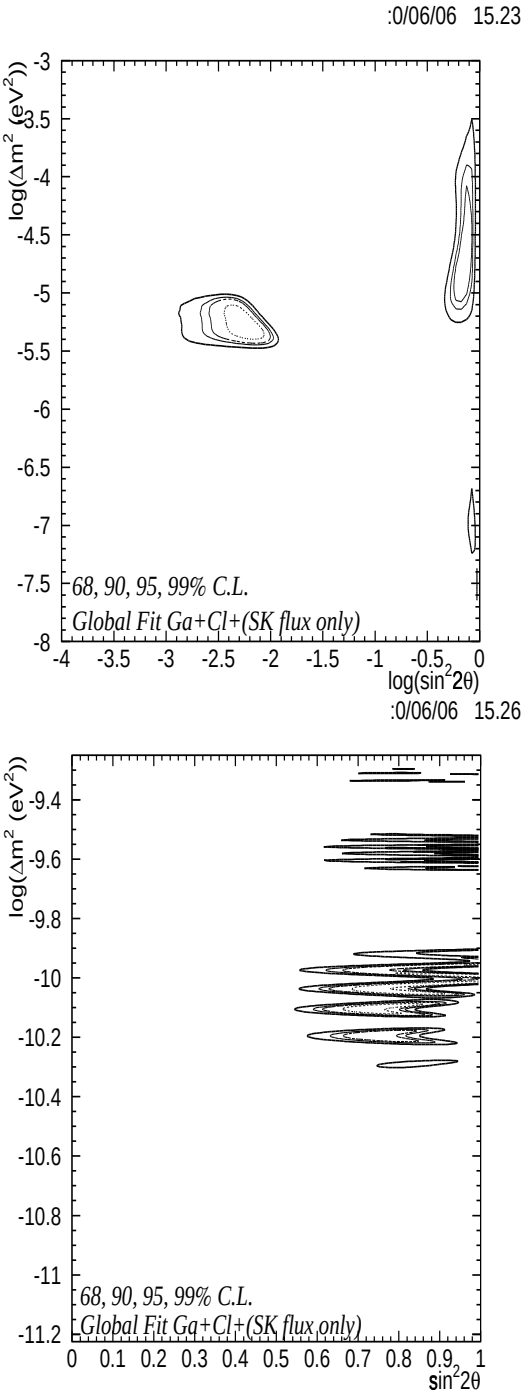

Figure 10. Allowed regions of oscillation parameter space using SK plus the gallium and chlorine experimental results and comparing to BP98.

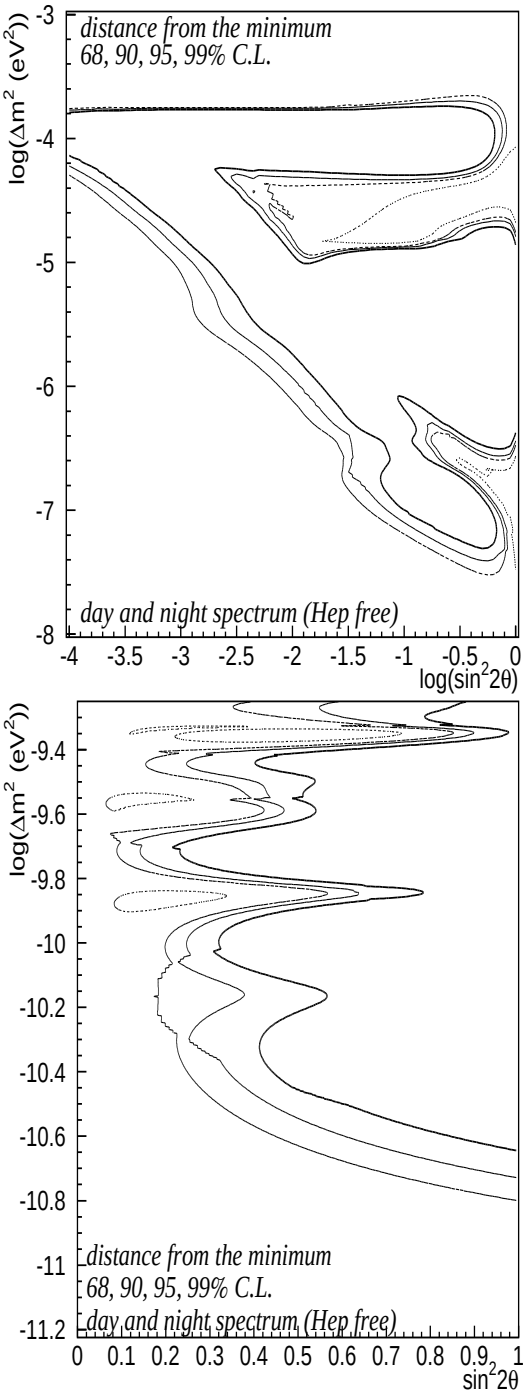

Figure 11. Excluded regions of oscillation parameter space using the SK solar-model independent measurements or energy spectrum and day/night enhancement. The normalization of the *hep* flux is taken as a free parameter.